Master RADMEP

Master of *Radiation and its Effects on MicroElectronics and Photonics Technologies* (RADMEP)

RECALIBRATION OF BEAM EVALUATION TOOL

Master's Thesis

Presented by

Alla Marchenko

and defended at

University Jean Monnet

9.9.2024

Academic Supervisor(s): Dr. Arto Javanainen, Dr. Frederic Wrobel

Host Supervisor: Françoise Bezerra

Jury Committee:

Dr. Arto Javanainen, University of Jyväskylä

Prof. Dr. Guy Meynants, KU Leuven

Asst. Prof. Dr. Matteo Ferrari, University of Jean Monnet

Assoc. Prof. Dr. Adriana Morana, University of Jean Monnet

With the support of the Erasmus+ Programme of the European Union

Université Jean Monnet Saint-Étienne

JYVÄSKYLÄN YLIOPISTO UNIVERSITY OF JYVÄSKYLÄ

KU LEUVEN

UNIVERSITÉ DE MONTPELLIER

Recalibration of Beam Evaluation Tool

Master's Thesis, 22.8.2024

Author:

Alla Marchenko

Supervisor:

Francoise Bezerra (CNES)
Arto Javanainen (JYU)
Frederic Wrobel (UM)

UNIVERSITY OF JYVÄSKYLÄ
DEPARTMENT OF PHYSICS

Abstract

Marchenko, Alla
Recalibration of Beam Evaluation Tool
Master's thesis
Department of Physics, University of Jyväskylä, 2024

Due to the harsh radiation environment in space the electronic devices may experience malfunction and even damaging effects caused by Single Event Effects. In order to verify the radiation tolerance of the devices, the test must be performed with a radiation beam before the mission. In order to obtain more reliable results of the test, the Beam Evaluation Tool was developed at CNES (BET-C). BET-C is designed to validate the particle energy and the distribution of the beam during the tests. The tool is utilising a position sensitive detector. The system is still under improvement after it was partially modified. Due to modifications, recalibration of the system was in order. Both energy calculation and position distribution had certain inaccuracies which were corrected by determining the calibration functions. The correction functions were established by using the non processed data extracted from the test campaign at UCLouvain where the BET-C system was tested under high energy ion beams. The results obtained with calibration function show considerable improvement in position distribution for all the ions. Regarding the energy, values close to the theoretical ones were achieved by using the data extracted from measurements with aluminium, chromium, nickel and rhodium. During measurements with carbon the position distribution was not detected and the raw signal that was obtained was too weak to include Carbon in the calibration. With xenon the upper limit of detection was reached leading to the conclusion that the optimal energy range for detection is between 250 MeV and 995 MeV.

Keywords: Master's Thesis, p-n diode, PSD, SEE, heavy ion testing, beam evaluation

Preface

I am absolutely grateful for the learning opportunity that CNES presented. It was a pleasure to work with wonderful people who welcomed me with kindness and introduced me to French culture. A special thank you to my supervisor, Françoise Bezerra, who patiently guided me through the internship, and to Marta Rizzo for her great contributions. Sincere thanks to my academic supervisors, Arto Javanainen, for his major contributions to the outcome of this project, and Frédéric Wrobel for his important insights.

I would also like to express my gratitude to the RADMEP master's program for allowing me to be a part of this amazing journey and for the opportunity to meet all the wonderful people who made this experience even more delightful. The professors I had the honor to learn from are outstanding experts in their fields and deserve special recognition.

Special thanks to my dearest friend Annika, who has been a great support throughout the university years and with whom I made unforgettable memories during this period. Deepest thanks to my better half Akseli, for providing constant encouragement and a shoulder to lean on. Last but not least, thank you to my family for their unconditional support, which helped me through these challenging yet rewarding years.

Alla Marchenko

Contents

1 Introduction

Performing radiation testing on electronic devices plays an important role in space mission success. The tests on radiation tolerance are performed by using radiation beams provided by the test facility. The properties of the beam are also provided by the facility. The beam used for testing devices may or may not be compatible with the standards provided by European Space Component Coordination (ESCC). For the verification of standards being fulfilled, the Beam Evaluating Tool, BET-C was developed by CNES, Centre national d'études spatiales which is the French national space agency. The system is designed to verify the energy of the radiation beam and the distribution of the particle flow. System was ready for testing in 2015 but the improvement process was still ongoing due to inconsistency in the measurement results. As the diode in BET-C was replaced with the similar one despite the limitations that were known. This decision was made due to incomplete characterizations of the diode, therefore no new technology was implemented.

During this work BET-C was tested at two test campaigns, one at TRAD and second one at Université Catholique de Louvain, UCL at the Heavy Ion Facility, HIF. test facility. The first limitations of BET-C were confirmed at a preliminary test campaign. At UCL BET-C was tested with high energy beams and data was collected with the BET-C system and with an oscilloscope. Unprocessed data that was collected with an oscilloscope allowed me to verify the inconsistencies between measured data with BET-C and post processed data and successfully recalibrate the system. The results that were obtained will improve the accuracy of BET-C in the future.

2 Context

Due to solar activity and other aspects in space the radiation plays crucial role in space missions. Even just one ionizing particle might cause permanent damages in electronic devices. The device testing must be performed and evaluated carefully before the mission.

2.1 Radiation effect on space electronics

In space, where Earth's protective atmosphere is absent, radiation poses one of the most significant threats for space exploration. The main radiation sources, radiation due solar activity, trapped radiation and cosmic galactic rays.

The Sun emits solar radiation driven by solar wind and solar flares. Solar wind is a continuous stream of charged particles, mainly electrons and protons, from the Sun's outer layer. This occurs when plasma is heated until the Sun's gravity can no longer contain it, leading to an expulsion of particles. When solar wind particles encounter Earth's magnetic field, they become trapped, forming the Van Allen radiation belts, densest around 2,000 km above Earth, consisting of high-energy protons and electrons [1]. Solar flares are sudden, intense bursts of energy on the Sun's surface that can cause coronal mass ejections [2]. The solar activity is proven to be in approximate cycles of 11 years when the activity reaches the peak when the magnetic field of the sun flips. When the magnetic field returns to its original state the so called Hale cycle is completed.[3]

In addition to the solar particles in space, Galactic Cosmic Rays (GCR), are present. GCR are high energy particles that mainly consist of hydrogen ions, protons, helium and heavy ions. The most significant source of GCR is the supernovae remnants. The particles travel through space at nearly a speed of light, from outside of the Solar System or other distant galaxies. These particles travel through space, influencing planetary environments and interacting with magnetic fields.[4]

As the size of technologies decreases many electronic devices experience disruptions during space missions. The malfunction of a device can be caused by a single particle

sometimes leading to permanent damage. These kinds of events are called Single Event Effects, SEE.

SET, Single Event Transient is the example of non destructive event when charged particles cause a temporary voltage spike in analog or digital circuits. Effect is usually short-lived but nevertheless can cause malfunctions in the device. SEU, Single Event Upset is another type of SEE that is not destructive. This event commonly affects the functioning of the memory cells causing a bit flips from 0 to 1 or vice versa. This effect can be usually corrected by rewriting the memory or by using error correction codes. Another possible effect that goes under the category of SEE is SEL, Single Event Latch-up, which can be observed in PNPN structure present in the CMOS technology. Unlike the SEU, this event can cause permanent destruction of the device. During SEL, the particle hit creates a short circuit between the power supply and ground leading to a high current in the circuit. If the current stays high for a longer period the device can struggle from overheating leading to permanent damage. Similar effect associated with power MOSFET is called Single Event Burnout, SEB, where the short circuit might create the high current that would lead to the damage. Single Event Gate Rupture, SEGR is the event when a particle causes breakdown of transistor gate leading to a short circuit as well. When the event is not associated with any of the previously mentioned categories it is Single Event Functional Interrupt which can be usually corrected by rebooting the system.

[1]

2.2 Radiation testing and beam verification

For successful space missions it is mandatory to perform variety of tests before the launch. Due to the radiation environment in space the radiation tolerance of the electronics on board need to be ensured. Either the devices need to be made radiation hard, or their radiation sensitivity need to be determined with testing.

The tests can be performed by irradiating the device with heavy ion, proton or gamma radiation beams. In this thesis we will mainly focus on testing with heavy ion beam and qualification of the beam used for the test. The facilities that provide heavy-ion beams for SEE testing are recommended to follow the criteria that is set by European Space Component Coordination (ESCC). ESCC provides a unified standardisation for component evaluation, qualifications and procurement. [5]

Regarding the fluence and flux of the beam it is stated that for testing with heavy ion or protons suitable LET and energy must be provided. More specifically the range in case of heavy ions must be at least 40µm in silicon and the flux should vary from 10 ions/cm^2/s to at least 10^5 ions/cm^2/s. Both fluence and energy must be uniform to ±10 percent over the area of the device under test, DUT. The facilities are not responsible for the adjustment of the energy and flux instead the user must consider the limitation while choosing the suitable facility. In addition to avoid contamination the ESCC requirements state that suitable vacuum must be provided implemented in the accelerator beam line. [5]

Regarding dosimetry, ESCC requires that the radiation dose should be monitored throughout the test and reported with an accuracy of ±10 percent. For accurate dose results of the position of DUT must be well known in respect to the beam. For heavy-ions the ionizing dose can be estimated using the Eq. 1.

$$D = F \cdot LET \cdot 1.6 \cdot 10^{-5}, \tag{1}$$

where D is a deposited dose and F is fluence in ions/cm^2 and LET MeV $\cdot$ mg/cm^2 . [5]

At CNES we are working on equipment that could verify the properties of the beam to be compatible with the specifications provided by ESCC. Beam Evaluation Tool, BET-C is capable of measuring the energy of the beam, flux, fluence and to visualize the location of the radiation particle hit to ensure the homogeneous distribution. As stated above the homogeneous distribution is required over the entire sensitive area of DUT.

3 Beam Evaluation Tool At CNES

BET-C is a Beam Evaluating Tool that is developed as a prototype at CNES. The equipment is used to evaluate the homogeneity and energy accuracy of high energy beams in order to verify the quality standards of the beam. Initially the BET-C system was developed in partnership with Institut de Physique Nucléaire d'Orsay, IPN, in 2014 by reusing the old position sensitive detector that was commissioned from IPN in 1990. The project included the development of BET-C head with IPN-PSD and preamplifiers that were added into the system. For the second part of the project BET-C rack was introduced. BET-C rack was responsible for acquisition of the signal starting from raw signal up to visualizing results with ADENEO software.

In 2015 the development of the system was finished and first tests were performed in order to evaluate performance of the detection head and acquisition rack both separately and together. The test results revealed a lot of inconsistency in BET-C. For the better understanding of the performance level of the system BET-C needs to be also tested with high energy beam which was finally possible in 2018. During this test campaign new challenges in the system were established but no modifications could be done due the unavailability of initial software developers and absence of required licence. Second test campaign was interrupted due the possible damage of the diode which was confirmed in 2019.

Later that year a new lot of PSD diodes were manufactured in IPN therefore the damaged diode was replaced shortly. Testing of alternative solutions and improvement processes continued until 2024. However, the long history of BET-C manufacturing and improvement brought a lot of uncertainty over the time due to loss of the original reports. The documents that were found are somewhere inconsistent which affect the improvement of the system. In this work the focus was on recalibration of the BET-C system with implemented new diode.

3.1 Position sensitive detector

Position sensitive detectors, PSD, are the type of detectors that allows not only the detection of ionizing particles but also the location of the particle hit. Position can be detected in one or two dimensions depending on the type of the detector. The working principle is usually based on the detection the generated charge and its density variation.[6]

3.1.1 P-N diode as particle detector

A P-N diode is a semiconductor that consists of two types of semiconductor materials, n-type and p-type. The structure only allows current to flow in one direction. The principle is to control the current flow by applying the external bias. The type of material is determined by the type of doping that is used. N side, or cathode, the negative side of the diode containing a high number of free electrons. The opposite side, which is the P side, or anode, has fewer valence electrons which creates the positive charge carriers that are called holes. When n-type and p-type of semiconductors are combined, the p-n junction is formed. In the middle between two semiconductors the electrons from n-side diffuse into p-side and fill the holes that p-type material contains. Holes travel to the n-side and combine with electrons respectively. The interaction between two type materials creates a depletion region between them which allows the current to pass in only one direction. Due to formation of depletion region there is a potential difference between the two materials. This potential difference is called built-in voltage. When the positive voltage is applied to the P side of the material, the forward biasing is created. This causes the reduction in built-in potential leading to decreased depletion region. That allows current to flow and increase exponentially with increasing forward voltage. On the contrary if the positive voltage is connected to the N side, the reverse biasing occurs therefore the depletion region is extended. During the reverse bias the current flow is negligibly small. Nevertheless if the reverse bias is critically increased it can no longer prevent the current from flowing which leads to reverse current through the diode. This is called junction breakdown which can be damaging for some diodes. [7]

The properties of p-n diode enable efficient detection of charged particles induced in the silicon layer. When the ionizing particle interacts with silicon atoms of the depletion region it causes inelastic collisions with electrons knocking them out of

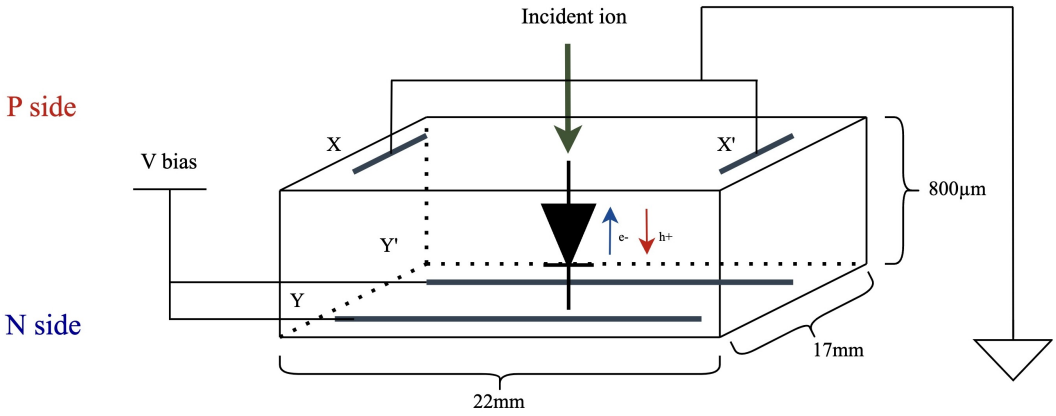

Figure 1. The structure of the diode.

their structure consequently leading to a creation of electron-hole pairs. The diode is typically reverse biased leading to an increased width of its depletion region where the concentration of free carriers is very low. The electric field that forms due to depletion region forcefully separates the electron-hole pairs followed by them drifting to either N or P electrodes. The movement of charge carriers creates the small current inside the diode which can be measured. Electrons are drifted towards the P side and holes towards the N side. The magnitude of the current that is created by the movement of charge carriers is directly proportional to the incident energy of the particle. This happens due to the higher amount of electron-hole pairs being created during ionization. Nevertheless, the current pulses that are induced are very low to be detected therefore they must be amplificated. From the detected signal, initial energy, position and the type of particle can be established depending on the type of the diode. [8]

3.1.2 BET-C diode

In this measurement system two layered Position Sensitive Detector, PSD, is used for estimation of the position of the beam [6]. The diode is a p-n diode that is reverse polarized. The diode is equipped with four gold electrodes, two on each side that are positioned in a parallel position to each other, which allows the collection of the charge at four sides X, X', Y and Y'. The structure of the diode is presented in the Fig. 1.[9]

The principle of charge collection in the BET-C diode is the following. Incident particle is deposited into a silicon layer causing ionization and consequently formation

of electron-hole pairs. The high voltage is applied to the N side of the diode for depletion, leading to a creation of the electric field inside. Due to the electric field, electron-hole pairs are forcefully separated. Hence negatively charged electrons drift to the electrode N that is located on the bottom level and positively charged holes to the electrode P that is on the top level of the diode. The drift of electrons creates current inside the diode which is detected by the electrodes. Depending on the distance the electron-hole pairs generated to the electrodes the amount of charge that is collected by the electrode will differ, therefore the intensity of the output signal will be different respectively. [9]

By using the information of distribution of the charge between electrodes it is possible to estimate the X and Y coordinates of the particles. When each particle is detected with a high enough sample rate and the position of it is calculated we can get the distribution of the beam. In order to detect the small signal change at the output, each electrode is connected to its preampliefier, therefore the signal gets amplified and converted to the voltage before propagating to the acquisition system. From Fig. 2 the structure of the detection head including the silicon diode and preamplifiers can be observed. [9]

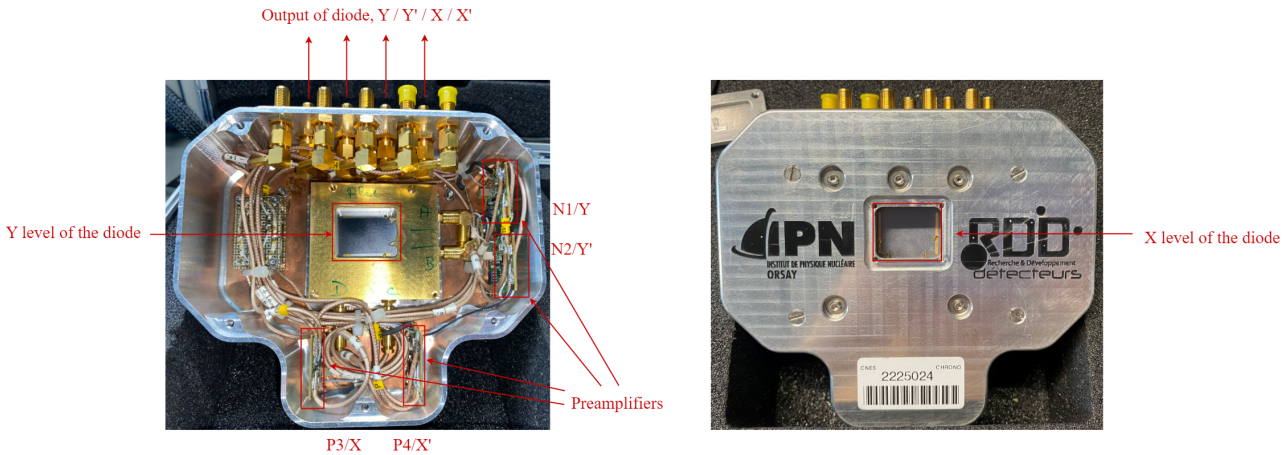

Figure 2. Detection head presented from back (left figure) and front (right figure).

In the Fig. 3 the schematic picture of the detection head is presented where the BET-C diode is observed in the middle and preaplifiers in the right as N1, N2, N3 and N4. The N side is connected to the bias and the P side to the ground since a reverse bias is applied. Via inputs Test N and Test P the diode is tested in real time in order to verify the proper functioning of the preamplifiers.[9]

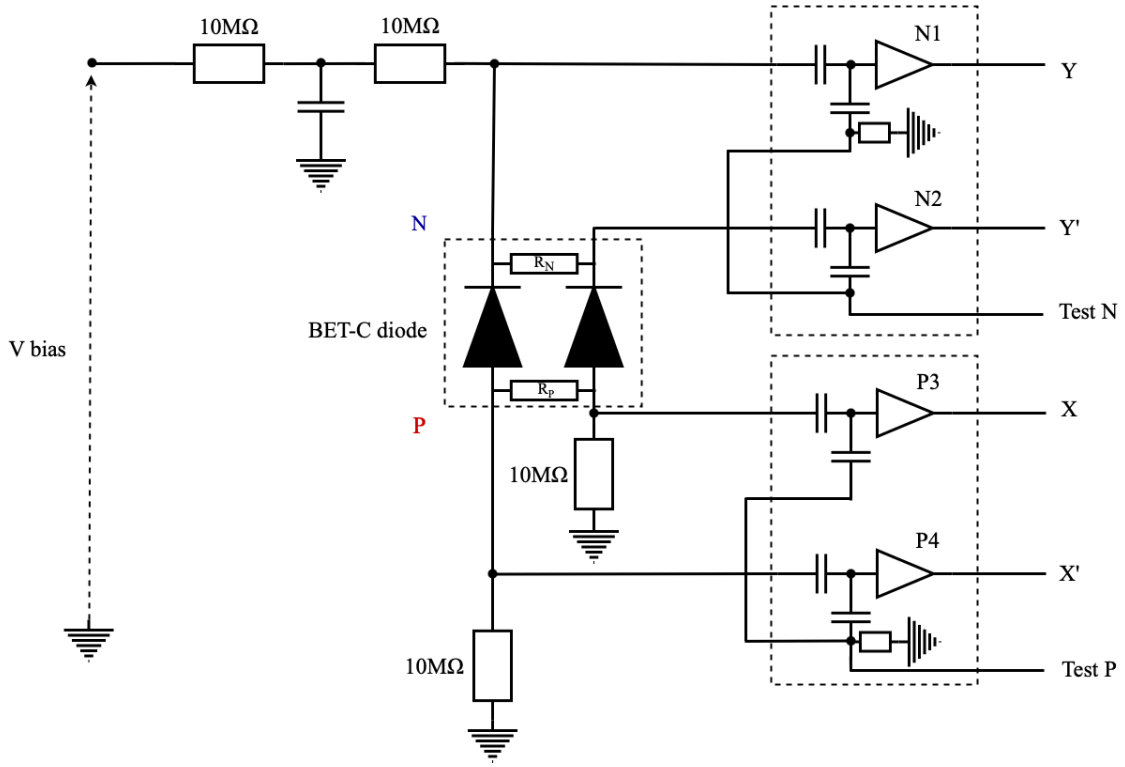

Figure 3. The schematic structure of the detection head.

Another important property that can be extracted thanks to the geometry of the diode is the incident energy of the particle. The incident energy can be back traced by adding together the two signals from each half of the diode and eliminating the impact of amplification system. [9]

3.1.3 Beam position

When the detector is depleted, it effectively detects the signal created by the charge movement at the first top with electrodes X or X' and at the bottom layer with Y and Y'. The location of the particle hit is calculated by using the signals that are collected from each electrode separately and inserted to Eq. 2 and Eq. 3. The equations calculate the proportion of the signal distribution by taking X and Y as main scale, consequently giving values between 0 and 1. In other word when the the particle strikes near X and Y electrodes the ideal location in coordinates is expected to be (1,1).[9]

$$P_X = \frac{X}{X + X'} \tag{2}$$

$$P_Y = \frac{Y}{Y + Y'} \tag{3}$$

3.1.4 Energy

When testing the devices for radiation hardening it is important to know the energy that the DUT is tested with. With the BET-C detector four signals from each electrode can be extracted and used to find the initial energy of the beam from the Eq.4 where E is the total energy extracted from both electrodes on the same level and E_{DL} is an energy that is lost due the dead layer on top of the diode.[9]

$$E_{tot} = E + E_{DL} \tag{4}$$

The energy loss of the dead layer E_{DL} can be calculated by using Eq. 5.

$$E_{DL} = \frac{dE}{dx} \cdot d. \tag{5}$$

Since the charge distribution happens equally on both the top and bottom layer ideally the energies of those levels are expected to be exactly the same. Nevertheless, in reality, this is not the case, therefore it is important to calculate both energies for the comparison and further investigation of charge distribution. For each layer, the energy, E can be calculated separately by using Eq. 6 and Eq. 7.

$$Energy_{1,2} = \frac{Y + Y'}{G_Y} + d \cdot LET \tag{6}$$

$$Energy_{3,4} = \frac{X + X'}{G_X} + d \cdot LET \tag{7}$$

In these equations X,X', Y and Y' are the edge height of the transients extracted from each electrode. The current signals generated in the diode are already amplified by the amplifiers and converted into voltage. [9]

3.1.5 Number of events

Each deposited charge represents one event that is counted in real time by the software. By knowing the number of events flux and fluence can be established. Following the formula 8 we can calculate the flux in real time that is dependent on the instantaneous number of particles. The area of the detector is $1.7cm$ x $2.2cm$.

$$Fluence = \frac{N}{A}, \tag{8}$$

where N is a number of particles and A is and are of the detector. And by using the same information as in previous formula we can establish the fluence by using the Eq. 9 where flux is integrated over the time, t_{tot}, therefore we get the total number of the events per area of detector over the specific amount of time.[9]

$$Flux = \frac{N}{A \cdot t_{tot}} \tag{9}$$

3.2 Acquisition model

After the signal is captured and amplified it is transferred to the acquisition system that is attached to the NI PXIe-1071 rack from National Instrument. The structure of the rack can be observed in Fig. 4. The acquisition system is directly connected to the output of the detector with 10 meters long wire in order to protect the rack from the effect of the beam when testing at high energy facilities. It has four inputs which allow to receive and store the data coming from the X, X', Y and Y' channels with sampling rate 120 MS/s. After that the data is encoded to 16 bits fragments and sent to the data processing unit. [9]

3.3 Triple power supply

For the proper functioning of preamplifiers it is mandatory to bias them with voltage. For that, the triple power supply is included in the rack. The voltage that is provided for the preamplifiers is +/-6V. Triple power supply is also responsible for biasing the silicon detector with high voltage in order to able the depletion of the diode. Triple power supply provides voltage between 0 to 20V and is connected to a DC/DC converter that converts the voltage to a high bias voltage that will be used to supply the diode. The range of the high bias voltage is between 0 to 1.1kV but for full

depletion of the current diode only 180V is needed. Triple power supply unit is presented in Fig. 4.[9]

3.4 Data processing unit

As mentioned before, all the signals are collected in the acquisition system where the data is encoded and then directly transferred to the data processing unit. The data processing unit consists of an FPGA module and a controller. The encoded data is first received by the FPGA for the processing where position distribution, energy and flux are calculated. The FPGA module that is programmed with LabView enables the continuous processing of data at the frequency of 40MHz when it is commanded by the controller.

The controller is an NI PXIe-8101 module that collects the calculated and processed data that is sent by the FPGA module in order to interpret and display the results. With the controller module triple power supply and the biasing of preamplifiers can be controlled. In addition, the acquisition rack includes a DMM module that measures the current that flows in the diode. In order to prevent the diode from damaging that high current would cause, the controller constantly checks that the current is below the threshold and alarms if the threshold is exceeded.[9]

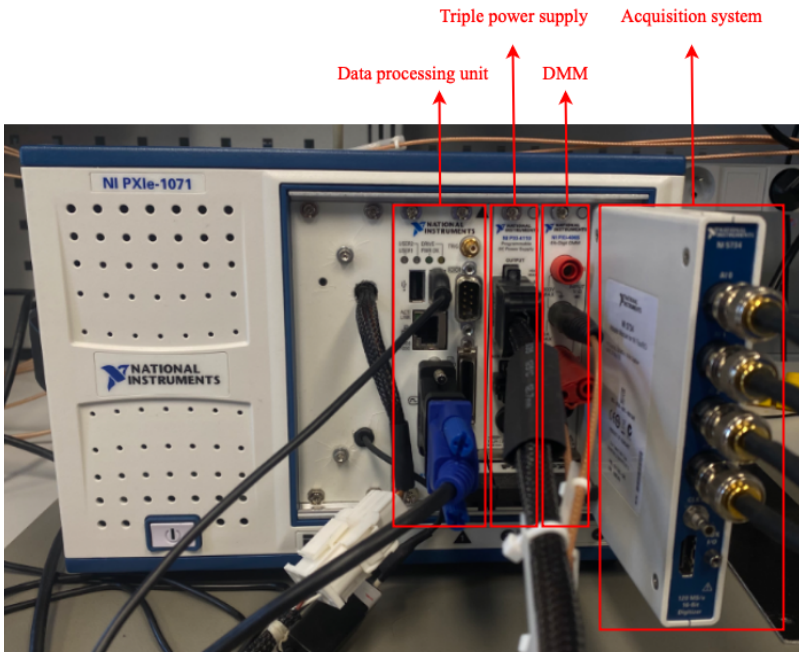

Figure 4. BET-C rack.

3.4.1 Software

Along the detector head, IPN developed a ADENEO software specifically for the BET-C system that would help to visualize results. Both software and FPGA are managed with the LabView therefore calculations and results can be managed simultaneously. Software is used to display the position distribution of the beam, energy, flux and fluence. Via the ADENEO software the polarization of the diode and power supply of the preamplifiers can be controlled. In the same tab we can control the current that is measured in diode in order to be alarmed if the threshold is being exceeded which can lead to diode disfunction.[9]

3.5 Upgrades

After the project of a BET-C continued the diode was replaced with a similar one manufactured in 2019 the needed calibrations were not implemented. As a result, the system is less accurate and results are not consistent. The goal of this work was to recalibrate the equipment and implement modifications for future measurements. For revealing the flaws of the system, two test campaigns were performed. During a first test campaign BET-C system was tested with a low energy source in order to find the detection threshold. For the second one the system was tested with high energy beams and raw data was collected for post processing.

The upgrades that require attention are the verification of the geometry of the diode that has been unclear due to inconsistency between reports and the visialization in software that might display the position of the beam incorrectly. If the error verifies, the modification will need to be implemented in software for beam distribution visualization.

Software often displays incorrect energy during measurement which can be the result of calculating it by using gains that were defined for the previous diode. By taking advantage of known energies of the beams that test facilities provide, the gain of the system can be recalibrated to obtain correct energy values in future measurements. Another possible issue to focus on is the position of the beam, since the beam distribution can be only tested properly with the high energy beams. During tests performed previously to this work some skewness was detected. The desired outcome of this work is the homogeneous position distribution, corrected with post processing in order to compensate for the skewness in detection.

4 Measurements

The development of BET-C was aimed for the high energy beams therefore two test campaigns were performed during this project. The goal of the test campaigns was to determine the upgrades that need to be done, and more importantly, to recalibrate BET-C rack for a higher accuracy.

4.1 Test Campaigns

The first test campaign took place at TRAD with a Californium-252 source that has an approximate energy of 5 MeV. The value of energy is provided by the TRAD.

The principle of BET-C diode is to collect the electron-hole pairs that are created when an ion passes through it. These carriers are collected by 4 gold electrodes distributed as follows: 2 on the top P side, 2 on the bottom N side. Therefore, the charges have to travel through the diode, from the location where they were created to the 2 layers and 4 gold electrodes. A particle hit is only qualified as an event when it is detected on both layers for the determination of position. The Cf252 source provided by TRAD is on the very limit of detection threshold due to the low energy of the heavy ions it emits by fission which leads to inaccuracy in detection.

First performed measurements with BET-C rack where the signal is processed by BET-C rack in order to see the response of the software. Four channels were connected to the acquisition system that is attached to the BET-C rack. The diode was placed into the irradiation chamber and connected to the system from outside. The irradiation was controlled by a shutter from outside that allows the exposure of the device to the source. All the measurements were performed in vacuum. In front of the diode a grid with 59 holes and a diameter of 0.1mm was used. The holes are distributed equally and the distance between each is 2.5mm.

The goal of this preliminary test campaign was to conclude the drawbacks of the BET-C system in order to prepare it for the next test campaign with high energy beam. In addition, we wanted to test the system with a low energy source in order to find the threshold of energy that would be still detected. Measurements were

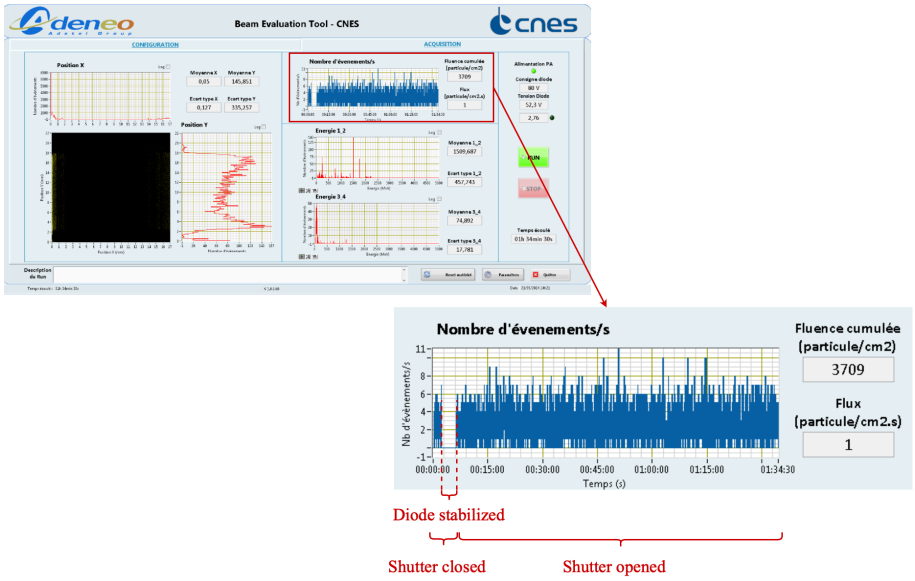

Figure 5. Figure represents the beginning of one of the measurements during the preliminary test campaign at TRAD. In close up we can see that the detector needs some time to get stabilized before the measurement can begin.

performed with two different polarization voltages, 80V and 100V. The detection threshold was changed in order to find the balance between noise reduction and pulse detection.

As a result of the test campaign it was concluded that the energy of Californium-252 source is too low to be detected by the BET-C system. With a low threshold of 10mV only the noise was obtained and with the increased threshold no signal was obtained. For the position distribution the signal has to be obtained from all four electrodes. Since the energy of the source was too low, the signal was only detected by the first level electrodes. Hence distribution was not seen. Nevertheless via particle count it was concluded that some particles were being detected.

From Fig. 5 it can be observed that the signal is only detected on one level of the diode, therefore the beam distribution does not correspond to the actual one. It can also be observed that the particle count in the beginning of the experiment is around 8 events per second, regardless of the shutter being closed. After a couple of minutes the particle count drops to zero and goes back up when the shutter is opened again. The experiment can conclude that the diode needs to be stabilized after the polarization before starting the measurement. In this particular run that is presented in Fig. 5, the stabilization time was approximately 3 minutes.

Stabilization is the time the diode needs for completing the polarization which is typically 150-200 ns. The BET-C diode is polarized gradually therefore the time to stabilize might be longer [10]. During polarization the charge is moving towards opposite electrodes creating the unwanted signal that disturbs the measurements. The intensity of the signal is close to a noise due to contamination in the surroundings. This measurement was performed in the vacuum, therefore contamination is minimized. This is also supported by Fig. 5 which shows that when the diode is stabilized and shutter is closed no signal is detected.

ADENEO software also displays the energy distribution of the source which in this case is expected to be around 5MeV. However, during the experiment the values for energy were quite unstable and well over the expected range. As an example the values of energy are displayed in Fig. 5 are 1509.687 MeV on top level and 74.892 MeV on bottom level. Therefore, it can be concluded that the measurements were not reliable. This is the consequence of charge not being detected on all four electrodes, leading to incorrect values of energy.

For the second campaign, the higher energy beams were needed. Therefore we travelled to Belgium to test at Université Catholique de Louvain, UCL at the Heavy Ion Facility, HIF. UCL provides some high energy beams, some of which were used for testing the equipment. Used ion beams are listed in table 1. For the test measurements were performed with 6 ion beams but for the recalibration of the system only aluminium, chromium nickel and rhodium were used.

Ion	Energy $[MeV]$	LET $[MeV/(mg/cm^2)]$	Range $[\mu m]$
C	131	1.3	269.3
Al	250	5.7	131.2
Cr	505	16.1	105.5
Ni	582	20.4	100.5
Rh	957	46.1	87.3
Xe	995	62.5	73.1

Table 1. List of ions that were used at the test campaign at UCL.

At UCL HIF facility BET-C system was tested with two test measurement configurations for each ion. In both configurations the diode is placed inside the radiation chamber and mounted onto the holder perpendicularly to the beam flow. Once the detector is mounted, the chamber is closed and the vacuum is pumped. In the first configuration, the diode was connected from the outside of the chamber

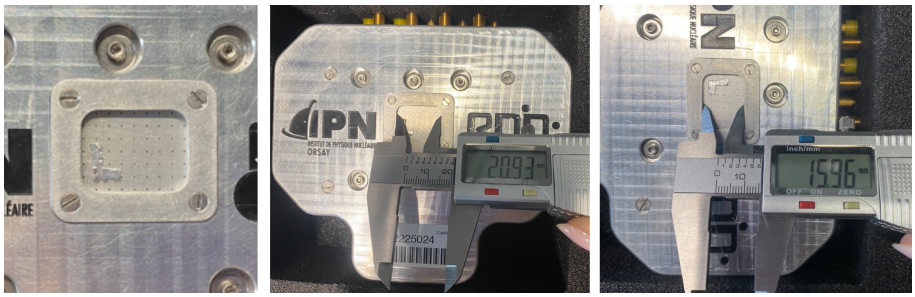

Figure 6. The properties of the grid that was use in front of the diode. On the left figure the L shaped tin foil shielding element used during measurement is presented. In the figures in the middle and right we can see that the grid is slightly smaller than the diode.

to the BET-C rack which allows us to modify the connection from outside during the measurements. In this configuration, all signal processing happens via internal acquisition system and visualisation with ADENEO software. For these measurements polarization voltages of 90V and 100V were used. The threshold was set between 10mV and 40 mV. For the second configuration the goal was to acquire the pulse data directly with oscilloscope in order to compare to results obtained with BET-C. The same way as in first configuration the diode was connected from outside of the chamber to the four channels of oscilloscope the same way it was in first configuration with BET-C rack. For the consistency of the measurements, also with an oscilloscope, 90V and 100V polarization voltages were used.

The goal of this test campaign was to collect data of a signal processed with BET-C system and to collect raw unprocessed signal that is collected directly from the output of the detection head with an oscilloscope for post processing. The results of BET-C and post processed results will be compared in order to recalibrate the internal data processing system of BET-C. From the previous test campaign it can be concluded that the energy range displayed with software was incorrect due to the low energy source that was used. Hence requires a confirmation if that would be the case with higher energies as well.

In front of the detector we used the grid previously shown that has 59 holes with a diameter of 0.1mm. The distance between holes is 2.5mm in each direction. In addition, part of the holes were covered with the tin foil shielding element shaped as L for asymmetry, leading to 55 remaining holes. This was done with the aim of visualizing the effect of different wiring configurations of the acquisition system. The properties of the grid are presented in Fig. 6.

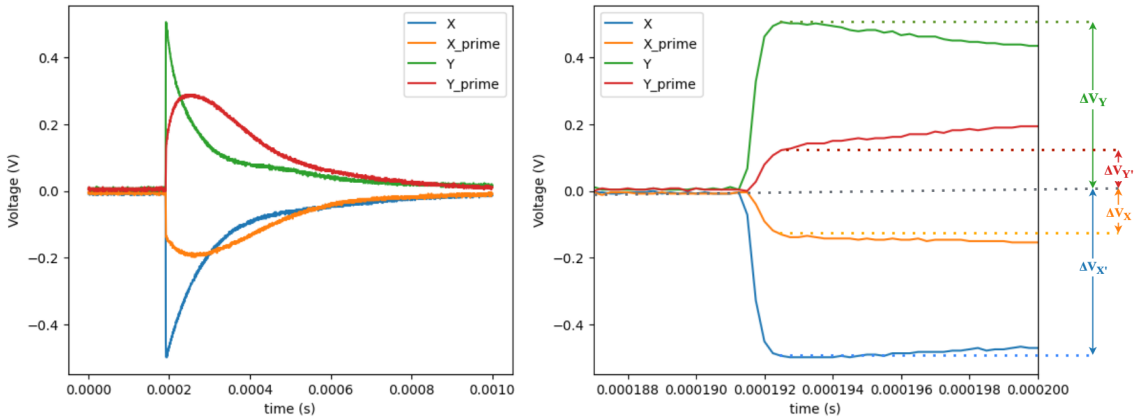

Figure 7. On the left we can see an example of a voltage transients measured with oscilloscope at UCL test campaign with nickel ion. On the right the same transient is presented as a close up with explained definition of a pulse edge height.

4.2 Data Processing

During the irradiation of the diode each event can be observed with an oscilloscope as transient voltage or pulse. Each event causes the ionization and eventually charge distribution across the electrodes. As a consequence four transient voltages are acquired. The response of each electrode is detected simultaneously, which can be observed in Fig. 7. Particles with higher energy will cause higher magnitude of the transients, as well as particles that hit closer to one or another electrode, since the majority of the charge collection will happen there. [8]

With high flux more activity can be detected, which leads to unwanted pile ups in the data. The pile ups are observed due to multiple particles striking on the diode within the decay time of a single transient leading to a recording of two particles as one single strike. That gives us unexpectedly high transient voltages, which increases inaccuracy in results. Possible examples of pile ups are presented in Fig. 8.

Since both energy and position distribution can be linked to the height of the transient, this quantity will be used as X, X', Y and Y' in calculation. However defining the height of the voltage transient, requires an adjustment to the shape of the pulse. At first the height was defined as the difference between the minimum value of the signal and maximum value, min-max approach. The voltage transient of the electrode that is located further away from the particle hit has a more round shape which brings the uncertainty to min-max approach due to the pulse rise even

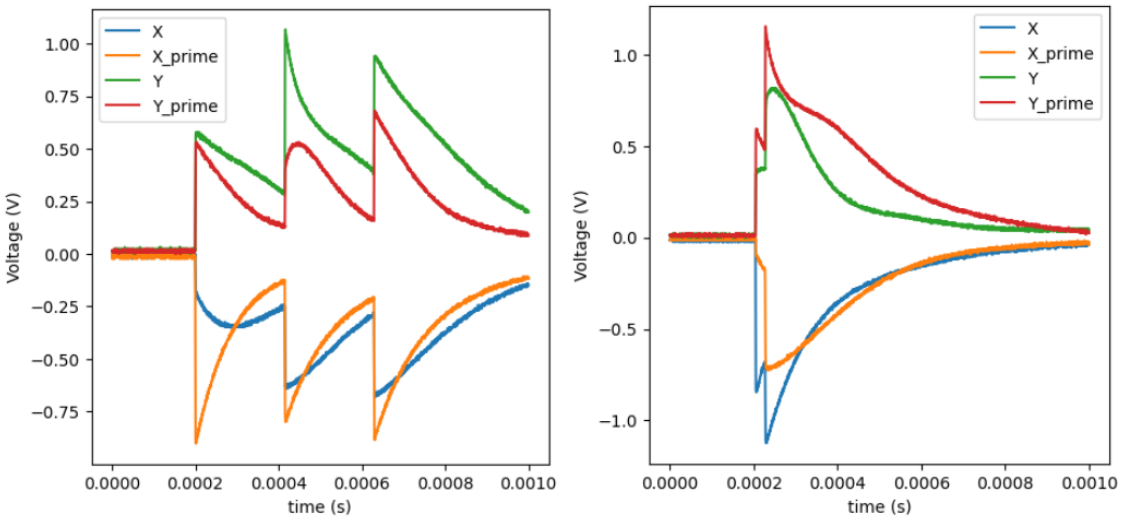

Figure 8. Possible distortion in measurements that are referred as pile-ups.

after the pulse edge has reached. That leads to the wrong interpretation of the magnitude of the pulse height and more skewed position distribution. In order to avoid that, a new approach was introduced. Instead of measuring min-max difference it was decided to measure the value of pulse height edge by defining the value of pulse height 1µs before the rapid increase and 1µs after. The definition of a pulse edge height is presented in the Fig. 7.

4.2.1 Energy Calibration

As the signal propagates from detector to the acquisition chain, it gets amplified by 4 preamplifiers, one at each output. The absolute gain of these amplifiers is not clearly documented, therefore the signal processing had to be recalibrated.

As the ion strikes into the silicon diode it creates the current inside it which leads to the collection of majority of the charge in the nearest electrode. The signal that propagates from the electrodes to the acquisition system is preamplified by the four amplifiers that are located inside the detection head. In addition preamplifiers convert the signal from current to voltage which can be then detected with BET-C system or oscilloscope.

When recalibrating the system, the whole detection head needs to be taken into account since it is impossible to measure the absolute gain of each amplifier. Therefore the energy calibration functions that are intended to find, describe the electrode detection, preamplification and signal propagation together. This will help

to calculate the initial energy from the signal that is received by the acquisition system.

In order to recalibrate the energy the calibration function needs to be determined. The Eq. 10 will be used in order to find the incident energy of the particle.

$$E = \frac{\Delta E_t}{\Delta h} \cdot h - E_0, \tag{10}$$

where E_t is the theoretical energy provided by UCL and h is the pulse edge height of the transient and E_0 is an offset.

As it is already established the charge generated by the ionizing particle distributes between electrodes depending on the physical location of the particle hit. Therefore the closer a particle hits to the electrode the higher voltage transient is expected. Because of that uneven distribution, the different signals collected on the P and N side of the diode needs to be considered, when establishing the transfer function. In the beginning of the analysis we started by filtering the transients with pile ups in order to not confuse pile ups for a very high transient voltage. False high voltage would affect the transfer function calculation by giving too high values leading to incorrect values for energy.

Now that the signal is filtered, we can calculate the pulse height edge of each transient from the four electrodes and add together the amplitudes of the 2 electrodes located on the same side of the diode, in other words $X + X'$ and $Y + Y'$. From the Fig. 7 it can be observed that the amplitude of each transient is measured from the zero point of the transient to the point when the pulse edge ends.

By calculating the energy calibration function by using total signal collected from electrodes on the same level the function that is compatible for both electrodes on level in question will be obtained. Determining the transfer function for each electrode separately is impossible since the signal distribution is unpredictable. Therefore, the signal amplification that is proportional to the energy of the beam cannot be seen. In addition for the gain calibration only 4 ion beams were used, which were aluminium, chromium nickel and rhodium due the inconsistency in the measurement results of the xenon beam. From the slope of the graph it can be determined the gain for X electrodes and Y electrodes and the offset from intercept. The calibration function that was determined by using all the ions is presented in Fig. 9 where the strong deviation is observed in the case of rhodium and xenon. Nevertheless for the energy calculation it was decided to exclude xenon. The calibration function based

on only four ions is presented in Fig. 10.

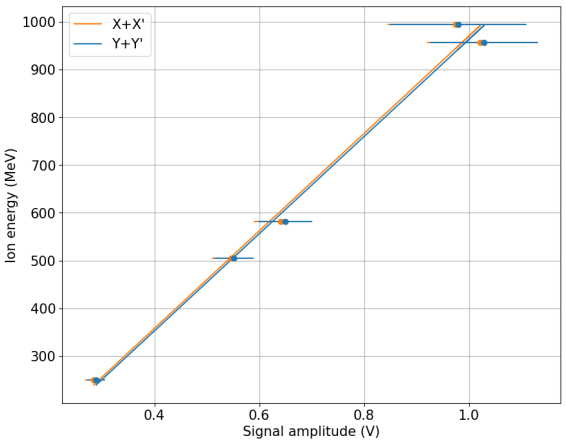

Figure 9. Energy calibration function with all the ions included.

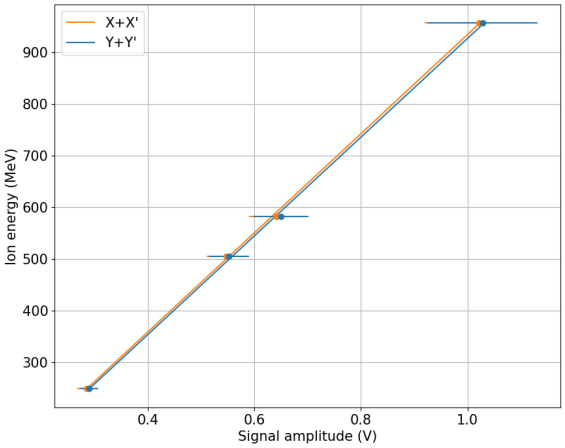

Figure 10. Energy calibration function with xenon ion excluded

	$G_X(\frac{MeV}{V})$	$E_0(MeV)$
X + X'	956 ± 14	-23 ± 9
Y + Y'	953 ± 16	-27 ± 11

Table 2. Fitting parameters for energy calibration functions.

4.2.2 Position Calibration

The position sensitive diode allows the visualization of a beam distribution in real time during the measurement. In this case, we use the distribution of a charge in order to determine the location of the particle hit. Each particle creates an event that causes the creation of an electric current inside the silicon detector. This current is detected by each electrode leading to a distributed charge collection. If the particle strikes closer to one of the electrodes the charge collection on that electrode is going to be more significant than on the others [8]. By extracting the raw data with an oscilloscope we can calculate the distribution of the beam by using Eq. 2 and Eq. 3 where X, X', Y, Y' are pulse height edges of the voltage transients.

The pulse height of the transient is directly correlated with the location of the particle strike. The closer the particle hits the electrode, the higher the expected transient. As an example five manually selected transients from detected particles are presented in Fig 11. In Fig. 11 (a), (b), (c) and (d) we can see that one of the

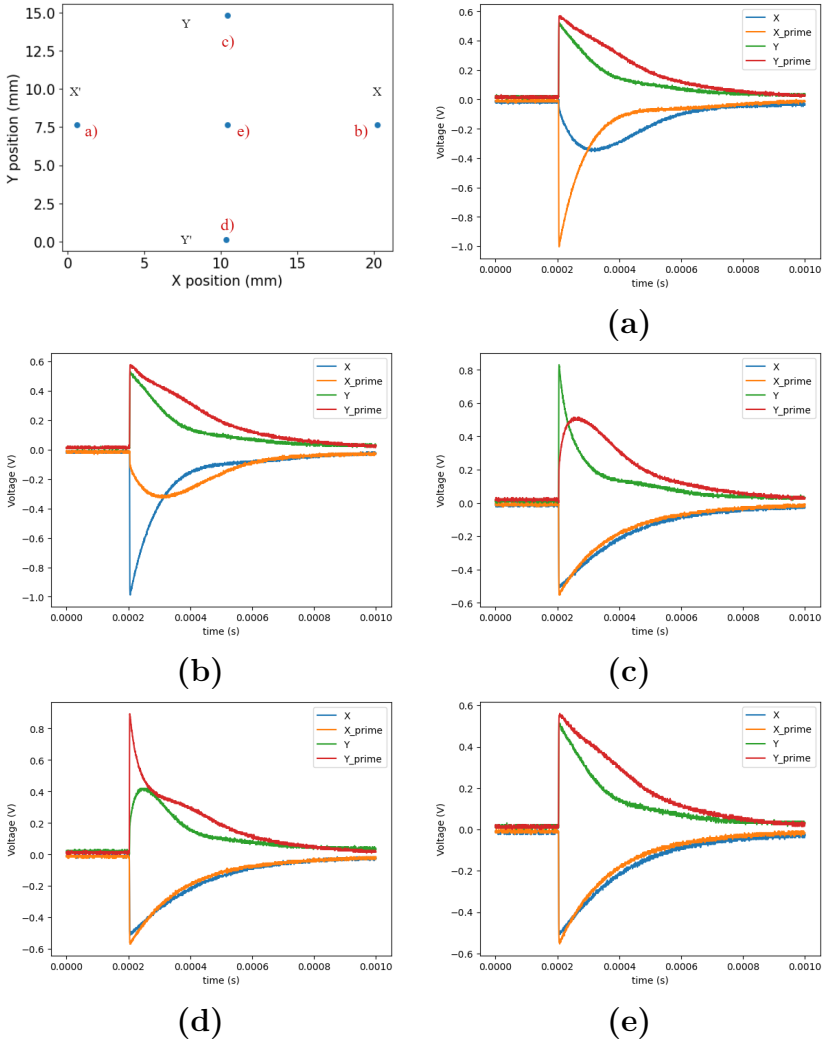

Figure 11. Representation of the position dependency on a height of the transients. The highest transient is observed at the electrode that is closest to the particle hit.

voltage transients is clearly dominating over the others. From that we can deduct that one specific particle hit happened closer to that specific electrode. In Fig.(e) all the transients are approximately equal leading to the conclusion that the particle must have been detected in the middle of the diode.

From the raw data that was extracted from the oscilloscope, the position distribution was calculated and presented in Fig. 12. Calculations were done by using Eq. 2 and 3 where the input values are pulse edge heights of the transients. The distribution is not scaled nor calibrated. For the comparison the same type of Fig. but estimated with min-max approach is presented in order to observe the improvement of using the pulse height edge instead of amplitude of the signal. In Fig. 13 the high skewness of the position distribution can be observed due to the uncertainty in defining the amplitude of the transient.

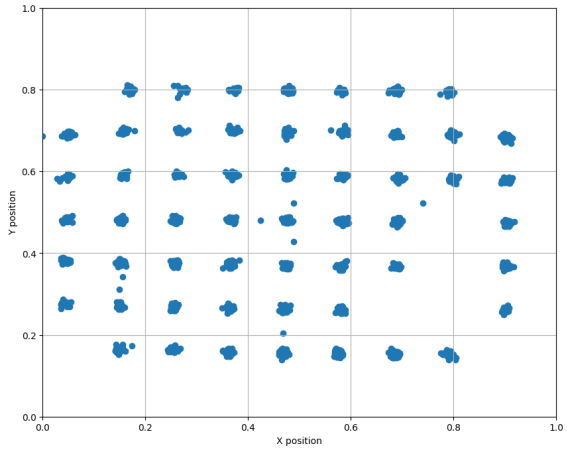

Figure 12. Non calibrated beam position on nickel.

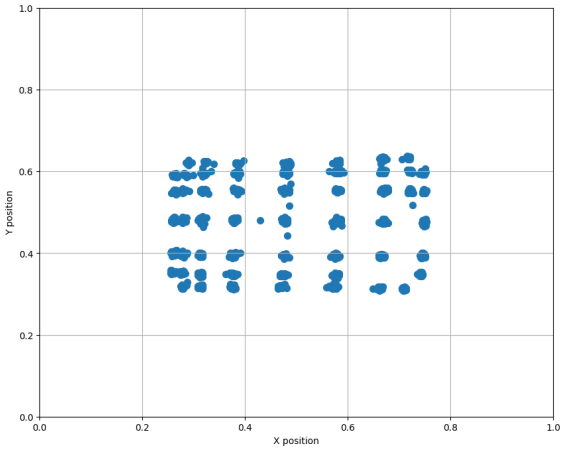

Figure 13. Non calibrated beam position on nickel with min-max approach.

The measured distribution of the beam is quite even, but it still has some scaling issues in both directions. However, the position is more shifted towards the centre in Y direction than in X direction. In order to see the actual distribution, we need to find the function that will calibrate the data points and set them according to the physical position of the ion strikes that is predetermined depending on the geometry grid in front of the detector. Because of the grid it is possible to recalibrate the position calculation in order to find the physical distribution.

Here, the possible method to correct the scaling issue for more accurate results is presented. For this calibration method, the data collected from measurements only with the nickel ion was used. According to a quick analysis, measurements with nickel have a low number of pile ups which would disturb the calibration. The energy of nickel is approximately in the middle of the detection range of BET-C diode, therefore it is the most optimal ion beam for the measurements.

From Fig. 12 it can be observed that the position distribution forms sort of a

cluster structure as a consequence of using the grid in front of the detector. For that reason the data points are now going to be treated in clusters, mathematically, in the data analysis as well. From the amount of holes in the grid we determine that there are 55 clusters and each one needs to be identified. For that the clustering algorithm was used that is called KMeans. The algorithm is used in machine learning and can be found from scikit-learn that is open source library for the Python programming language.[11]

The idea behind the Kmeans algorithm is to find clusters numerically by first assigning the centroids randomly. The amount of centroids can be predefined depending on the dataset. In our case the number of clusters is 55 therefore we define 55 random centroids. Then the algorithm calculates the distance from each centroid to each data point by using the Euclidean distance and assigns points to the nearest centroid. After all the data points have been assigned to a centroid and its corresponding cluster, the coordinates of each centroid is recalculated by averaging all the points in the cluster. Then, the whole process is repeated until the centroids no longer move. [11]

Once each cluster is identified, centroids for each one can be assigned. The clusters and their centroids are presented in Fig. 14. The reason for finding the centroids for each cluster is that we need to assign each one to the correct physical position that is, again, predetermined via geometry of the grid.

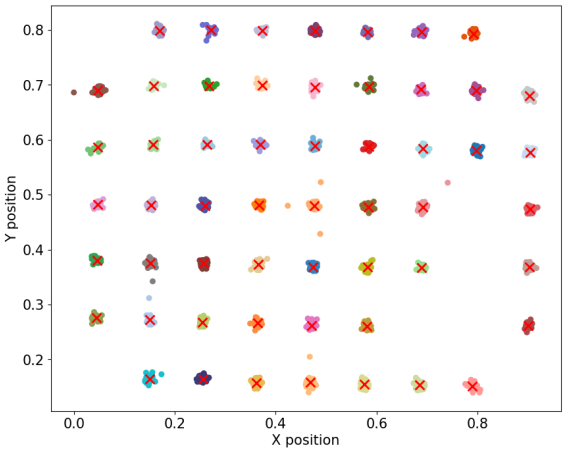

Figure 14. Centroids identified with KMeans algorithm and presented as red crosses.

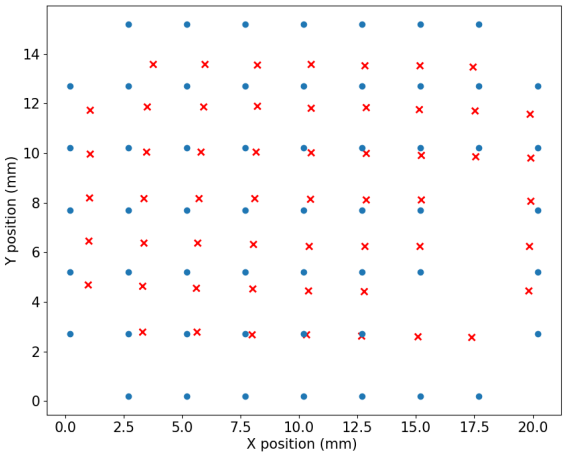

Figure 15. Centroids scaled simply using the diode size in comparison with the physical position.

The grid that is used for this measurement is smaller than the size of the diode

and has 2.5mm of distance between the holes in both directions. The size of the diameter of the holes is approximately 0.1mm (See Fig.6). In the Fig. 15 it can be observed that the position distribution of the centroids compared to the physical position of the grid holes. In order to get the distribution that corresponds to the physical geometry of the grid coordinates of centroids are simply multiplied by 17mm and 22mm which is the area of the diode. The grid holes presented in the figure do not correspond to the size of the actual holes. For asymmetry of the position distribution the L shaped area was covered in the right corner which can be also observed in Fig. 14 and 15

From both Fig. 14 and Fig. 15 it can be observed that the data points are shifted in both directions. Ideally the distribution of the beam should be between 0 and 1 which is not the case in Fig. 14. The same effect can be observed in the Fig. 15 which illustrates clearly the higher shift in y-direction than in x-direction.

In order to correct the shift we need to determine the position calibration function that would establish the correct position for all the data points. To determine the function, we will use the coordinates of the centroids that will represent all the data points in its cluster.

We start by finding the dependency of the real position on the observed corresponding one by plotting the graph where expected physical position is a function of the observed one. That way, when the values of the observed position are passed to the function as an output, the corrected coordinates will be obtained. For both directions x and y independent functions need to be established. The graphs of the position calibrating functions are presented in Fig. 16 and Fig. 17.

For these data points the linear functions can be fitted, that would shift the data points into correct locations. The parameters for both graphs are presented in a table 3.

$$P = S \cdot P_{observed} - P_{offset}, \tag{11}$$

where S is a slope of the graph and P_{offset} is an intercept. Now that the fitting parameter are found, the correction functions for X position and Y position can be presented.

In order to implement the correction new coordinates need to be calculated for X and Y positions by using the correction function. The results of calculated new positions are presented in Fig. 18, where blue dots are the measured and calibrated

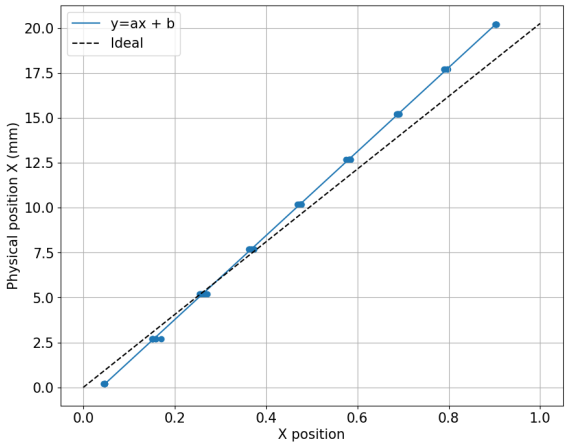

Figure 16. Position calibration for distribution in x-direction

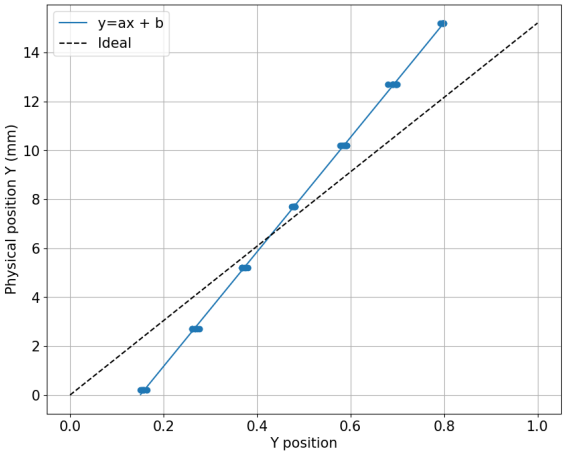

Figure 17. Position calibration for distribution in y-direction

	S	P_{offset}
P_X	(23.39 ± 0.05)	-0.91 ± 0.03
P_Y	(23.41 ± 0.07)	-3.51 ± 0.04

Table 3. The fitting parameters for position calibration functions.

data points and the red crosses are the distribution of physical positions. Ideally the slope of the graph should be around 22 and 17 therefore it can be seen from the observed slopes that position is shifted towards centre.

By using the position calibration function new positions that would correspond to the real positions are calculated In the Fig. 18 calibrated position is presented for the nickel ion beam distribution along with the real position that is indicated by red crosses. This confirms the efficiency of the correction function implemented.

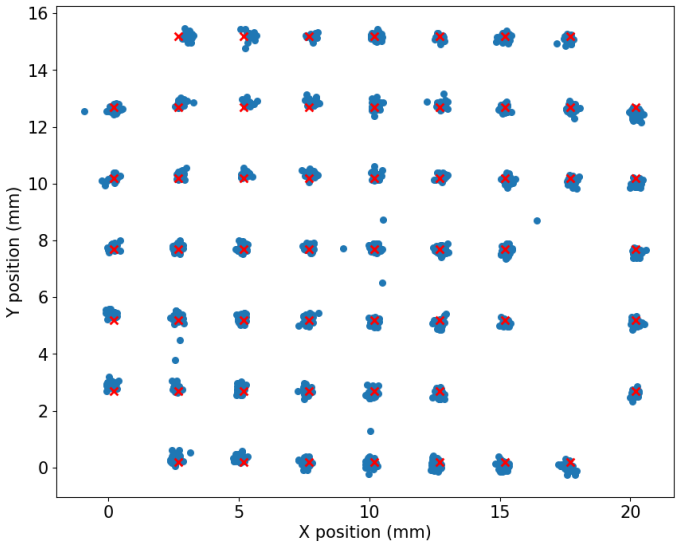

Figure 18. Recalibrated position of nickel beam with comparison of the real position of the beam illustrated as red crosses.

4.2.3 Correction on geometry of the diode

The diode that is used in the detection head behaves like a PN detector where the P doped side collects electrons and N doped side holes. With the BET-C rack we do not have access to the raw data, therefore it is impossible to confirm the geometry with measurements based on BET-C system results. At UCL, the behaviour of the diode was tested with an oscilloscope collecting non processed signals from the four channels.

As it was previously known, the diode has P and N faces that contain holes and free electrons. When the diode is polarized in reverse mode, the depletion region between its two faces increases where holes and electrons tend to diffuse into opposite sides [7]. During the measurement when the incident particle causes the ionization in the silicon diode the negative charge carriers drift to the P side and the positive to the N side which will lead to a negative output signal on P side and positive output signal on N side.

From oscilloscope measurement four signals were detected from which two were negative and two positive. By backtracking the propagation of the signal from each electrode up to the acquisition system, we established that the P face indeed belongs to X and X' level and N face to Y and Y' level. We were also able to see that the P face is on the top of the diode and N face is on the bottom.

4.3 Results

Both energy and position required calibration, both of which were performed in order to implement them for the future measurements. For the energy calibration it was decided to use only the data obtained from the measurements of aluminium, nickel and chromium beams, due to unexpected inaccuracy in measurement results with carbon, rhodium and xenon. From the results the graphs were extrapolated, which needed to be compatible for energy calculation including higher energy beams. For the position calibration only used data extracted from measurements with the nickel beam was used. Therefore, in this chapter, the results after implementing the same correction function to the rest of the ions are presented.

4.3.1 Energy

One of the relevant features of the BET-C system is that it is capable of measuring the energy of the radiation beam. As the signal distributes between electrodes we can find this energy by adding the signals acquired on a given side of the diode back together, and eliminating the effect of amplification by using the gain calculated earlier. When a signal propagates it is amplified and converted, therefore we need to back trace the initial energy by compensating these effects of preamplifiers. In practice the calibration was made by first finding the pulse edge height for each transient that is detected with each event. The pulse edge heights were presented in the graph with their corresponding energies. The data point formed a linear dependency to which the function was fitted. The graph of the gain can be observed in Fig. 10. For the energy calibration it was decided to exclude the xenon due to highly inaccurate measurement results that can be caused by a random error. Therefore the calculations were made with the help of a calibration function that does not include contribution of measurements with xenon. The results extracted from the measurements with xenon are discussed more precisely on Chapter 5.

Now that the calibration function is found the initial energy of the particle can be calculated. Ideally the values for the energy are expected to be the same as the theoretical ones but due certain deviation in the graph the results have slight uncertainty. In the Table 2 we can see the parameters for the energy calculation which were used in order to obtain the values presented in Table 4. Energies on both layers were calculated from Eq. 6 and Eq. 7. In the equation it is stated that the

energy loss caused by the dead layer has to be subtracted. However the dead layer is claimed to be negligible therefore it is not taken into account. Nevertheless from the energy value the offset needs to be subtracted. The offset includes information about dead layer energy loss and the LET of the particle. In the equations we use the edge height of the signals that are extracted with an oscilloscope from each electrode X, X', Y, Y'. As a result we obtain the energy distribution formed from each particle strike. The energy distributions for the X layer of the diode is presented in figure 19. In the Table 4 the most frequent values are presented or in other words the energy that most particles had. Regardless of the decision to leave xenon out of the calibration process it was still possible to calculate the energy of it therefore all five ion energies are presented.

Ion	**Theoretical energy (MeV)**	**Pulse edge height approach**	
		Energy X (MeV)	Energy Y (MeV)
Al	250	250	254
Cr	505	508	509
Ni	582	608	606
Rh	957	985	991
Xe	995	953	949

Table 4. Ion energies calculated by using the energy calibration function for X and Y.

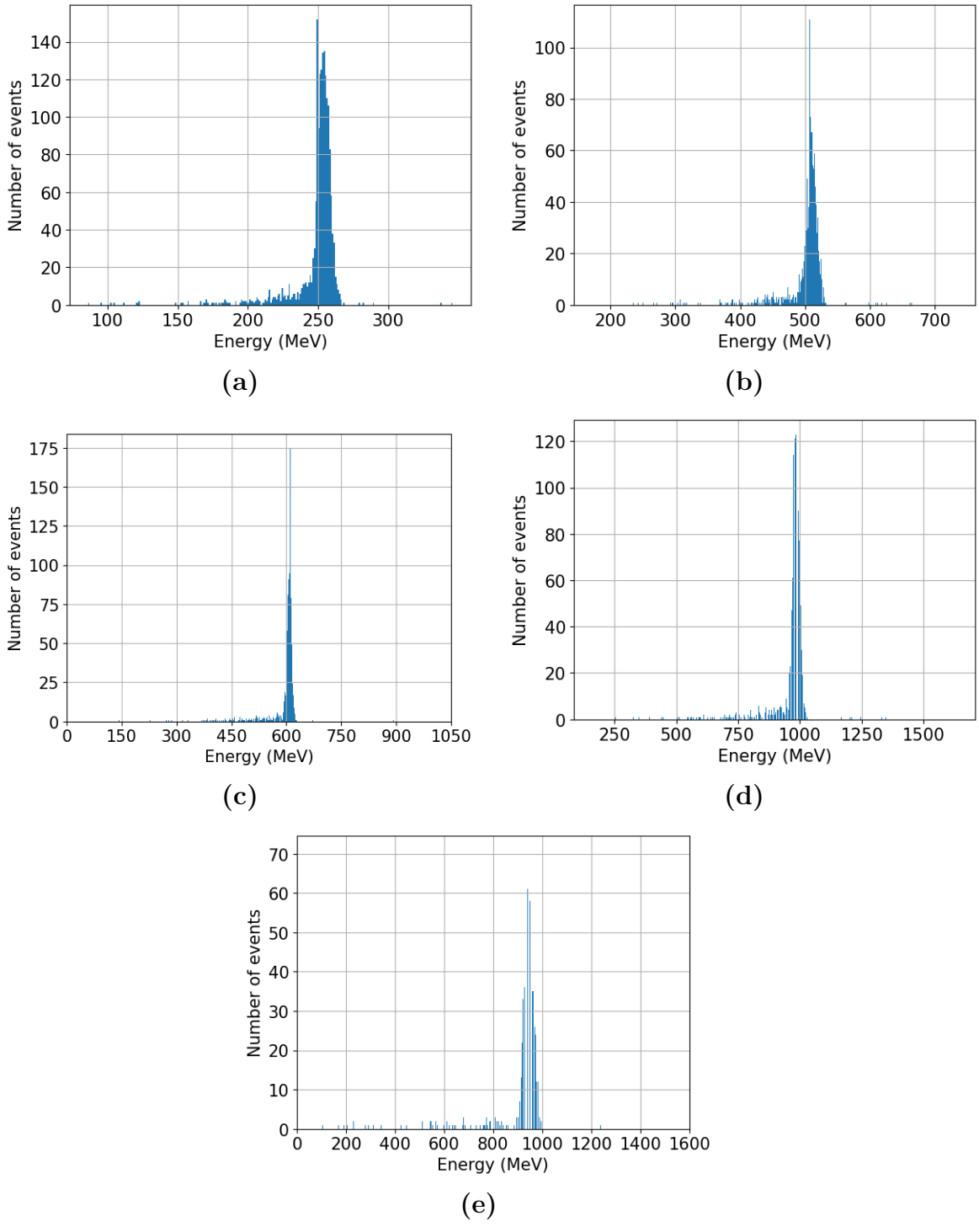

Figure 19. Energy distribution of the charge that were collected on X level of the diode. **(a)** Energy of aluminium. **(b)** Energy of chromium. **(c)** Energy of nickel. **(d)** Energy of rhodium. **(e)** Energy of xenon.

4.3.2 Beam position

As mentioned earlier during the test campaign the measurements were performed with the BET-C rack where data processing happens internally in real time and with an oscilloscope from which the raw data was extracted and post processed. The results obtained with BET-C rack and visualized with ADENEO software are presented in figure 20. All the ions in the figure are measured with a polarization voltage of 100V. From the Fig.(a) it can be seen that for the carbon ion beam the signal was not detected at the bottom layer therefore the position distribution is not observed. In case of aluminium Fig.20(b) and chromium Fig.20(c) it is possible to detect the distribution but the visualization is very low due to low charge collection on the bottom level. The higher the energy the more intense is the position distribution which can be observed in remaining figures. The position distribution varies depending on the measurement run due to different order of the wire connections. In order to see dependency of the wire connection and position some holes were covered asymmetrically with an L shaped block, Fig6. That way we can establish that switching X and X' wires will flip the position in lateral direction and switching Y and Y' wires in vertical. If both wires X and Y are switched with each other the image that is presented in Fig.20(e) can be observed, where position is rotated in 180 degrees.

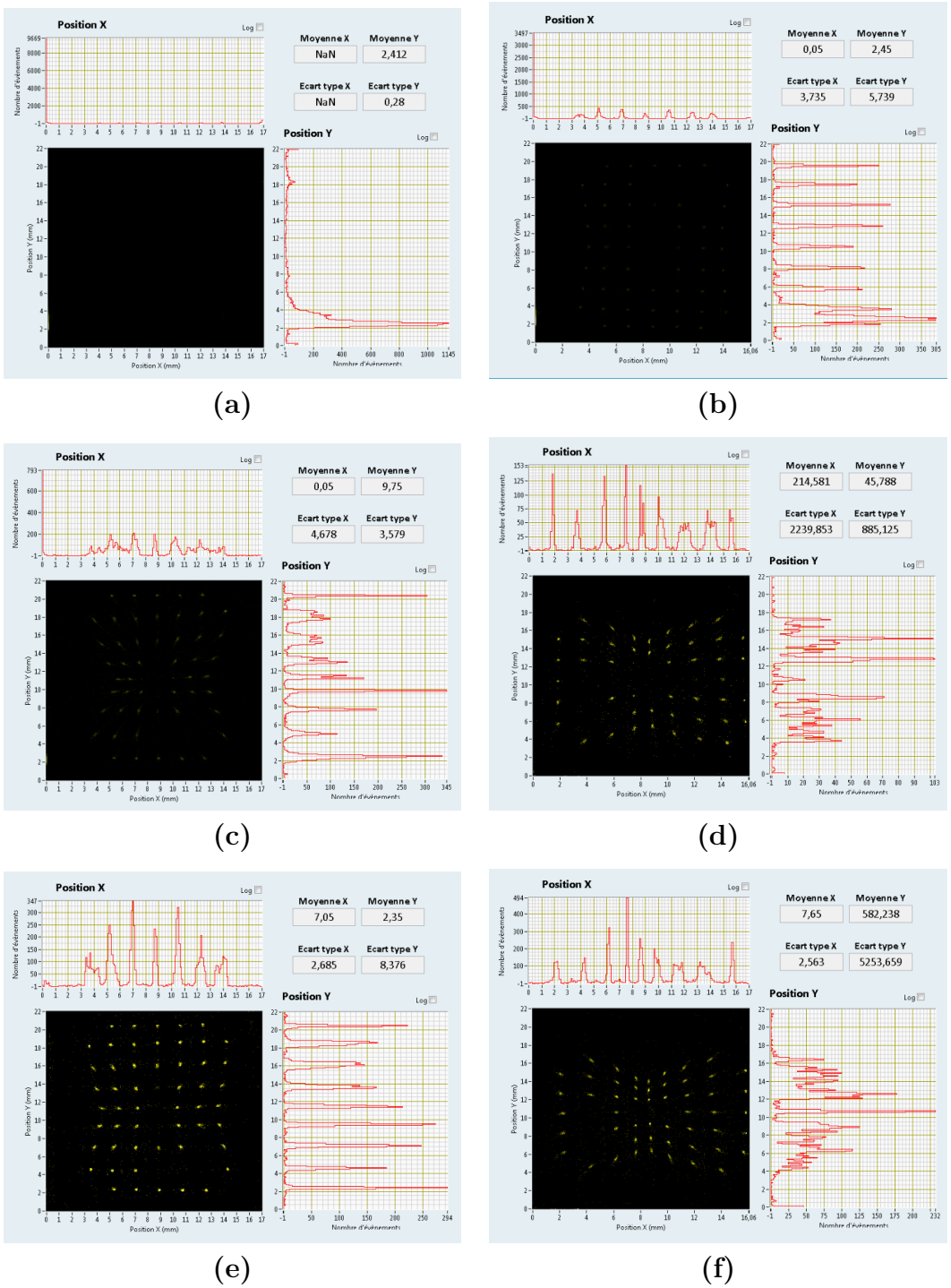

Figure 20. Position distribution detected with BET-C.**(a)** With carbon ion beam distribution was not detected. **(b)** Low detection with aluminium ion beam as well. **(c)** The beam position is becoming more visible with higher energy. The position distribution can be seen with chromium ion beam. **(d)** Position of nickel beam with wires connected in different order. **(e)** Position of rhodium beam where order of the wires is changed again. **(f)** Position of the xenon beam.

In the Chapter 4.2.2 the way to find the calibration function was presented. For the calibration it is sufficient to use the data collected from only one ion beam. For the calibration the most accurate result should be picked and in this case it was nickel. With nickel beams the least amount of outliers were observed. Initial position calculation before calibration were performed by using Eq.2 and 3 where again X, X', Y, Y' are the pulse edge height. With the position distribution of the nickel beam the dependency to the real position was found and presented as a position calibration function in Eq.11. After establishing the calibration function the new positions were recalculated and presented in Fig.21.

The ideal distribution of the beam would have the physical parameters of the grid that are noted in Fig. 6. The distance between the holes are approximately 2.5mm and the holes are distributed between 22mm x 17mm area. As mentioned, nickel has the least amount of outliers unlike the ions with higher energies like rhodium Fig.21(d) and xenon Fig.21(e). The reasons for that are discussed in Chapter 5. Also in case of aluminium Fig.21(a) the distortion in position is observed at the left side.

After the calibration of the position the distance between the calibrated position and the real physical position that is determined by the grid were calculated. The results are presented in the table 5. The lowest value is observed for nickel since the calibrations were made with nickel ion beam data. The value is higher the further the energy is from the nickel energy but distribution is relatively low.

Ion	Energy (MeV)	Distance (mm)
Al	250	0.233 ± 0.003
Cr	505	0.213 ± 0.003
Ni	582	0.189 ± 0.002
Rh	957	0.208 ± 0.002
Xe	995	0.229 ± 0.004

Table 5. Average distance between calibrated data points and the real position that was expected from the measurements.

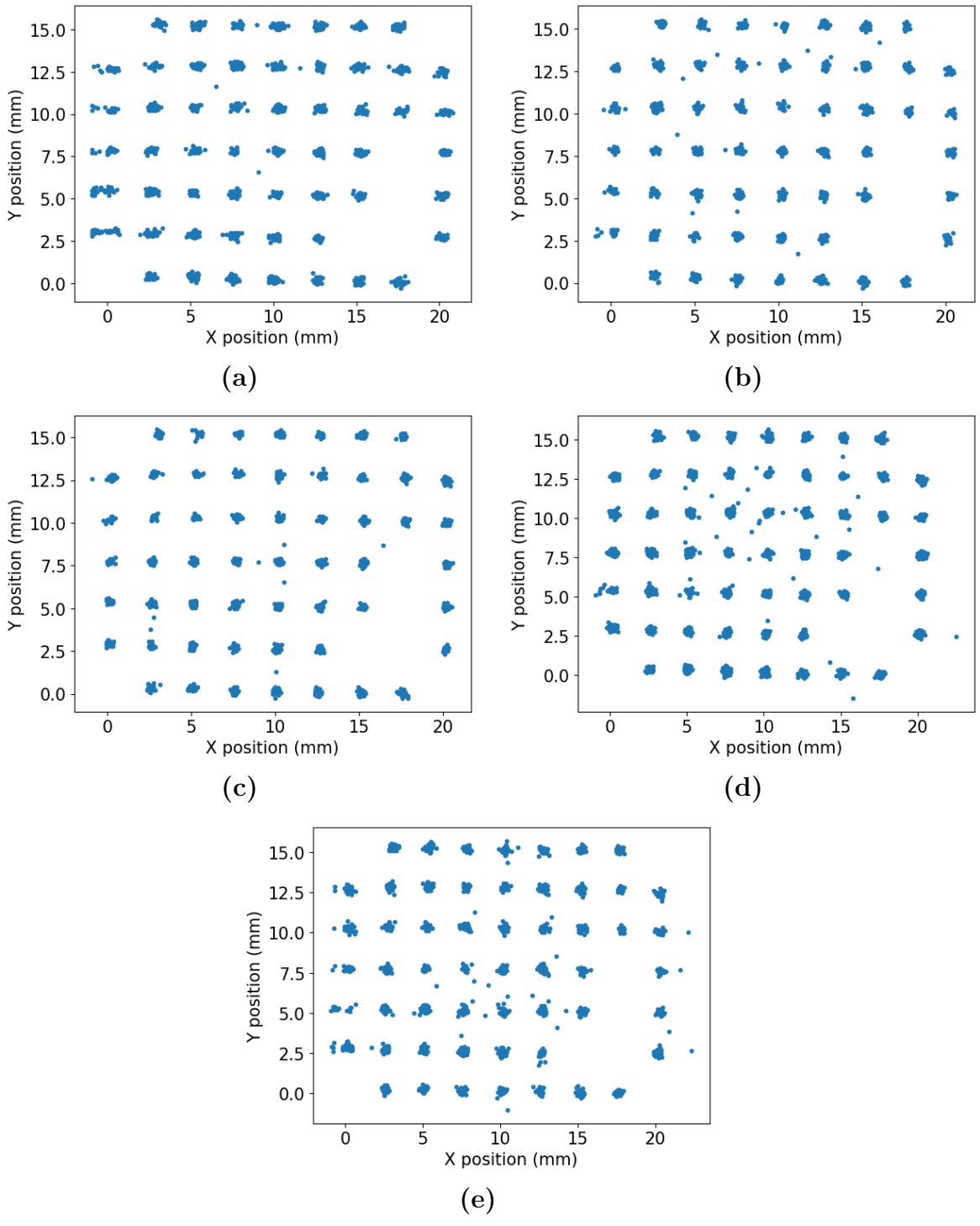

Figure 21. Calibrated position of each ion by using the position calibration functions for x- and y-coordinates.**(a)** Beam position of aluminium. **(b)** Beam position of chromium. **(c)** Beam position of nickel. **(d)** Beam position of rhodium. **(e)** Beam position of xenon.

5 Discussion

The project of BET-C was put on hold due to a lot of inconsistencies and errors in data processing. Since the project was started a long time ago and suffered turn over from the ADENEO company in charge of developing the rack and the attached software, a lot of information of the structure and performance of the system are still unclear. As a result of this work it was managed to recalibrate the data processing of the system along with retracing geometry of the diode that is currently used in the BET-C system. The verified geometry of the diode is presented in the Fig. 1 where we can see that the beam arrives at the P face of the diode where electrons are collected and holes are collected on the N face of the diode which is located at the bottom.

Due to the thickness of the diode, which is 800µm, there are some detection restrictions involved. From the Fig. 7 signals that are extracted with the oscilloscope from all four channels can be observed. Two of those signals are higher which indicates that the particle strike was closer to those electrodes than the opposite ones. For the electrodes that are further away from the particle strike, we can see that the voltage transients are significantly lower and have a more round shape. The phenomena that can be observed is due to the attenuation of the signal due to the long travel distance of the carriers. When the signal travels through the diode some of the charge may recombine, thus resulting in amplitude attenuation for the collected signal [12]. In addition, due to high energy the flux is high as well which leads to an accumulation of charge in the detector. Detector can become saturated with charge carriers leading to a reduced efficiency of a charge collection and weakening of a signal at the output. [13]

5.0.1 Energy range limitation

In the calculations of the transfer function both electrodes on each of the X and Y planes are taken into account, leading to the same value for gain and energy loss of the same level electrodes. This is mandatory due to the distribution of the signal. Since the distribution depends on the location of the particle hit, that makes it unmanageable to control the intensity of the signal that is being detected on each electrode. However, the total intensity of the signal is always the same and expected to be similar on both layers. Therefore it is the quantity that can be linked to the deposited energy. The intensity of the signal is directly proportional to the deposited energy and the increase is linear as presented in Fig. 9. Nevertheless, inaccuracy in a linear fit can still be observed. The inaccuracy can be caused by the recombination of electron-hole pairs leading to a partial signal loss [12]. Since the function that is fitted to the data points is used to verify the initially deposited energy, some deviation can be seen in these results as well. All the calculated values for energy are within the error margin.

After careful examination of the measurement results, inconsistencies were found for the xenon for which the calculated energy is lower than expected and lower than the one of rhodium. It is assumed that the signal created by an ionizing particle is directly proportional to its energy. In case of all other ions the energy that was calculated is within error range, that is presented in Table 2 except for the xenon which is 937 MeV - 942 MeV. The value is too low compared to the value that is provided by the UCL HIF test facility which is 995 MeV. The inconsistency can be explained by taking into account detection limitations of the diode. The theoretical detection limit that is provided by the manufacturer is approximately 1GeV which is very close to the energy of xenon.

Measurements were also done with a lower energy range that was provided by a carbon beam. The run performed with carbon ios, however, was cut short for the operational reasons, therefore there was not enough data to provide applicable results. For this reason carbon data was left out of calibration as well. Measurements with BET-C showed that no signal was detected on the bottom side of the diode, therefore calculation of position distribution was impossible, which can be observed in Fig. 20. As it was established earlier, the energy of the beam is directly proportional to a signal that electron-hole pairs create. When the concentration of electron-hole pairs is low, fewer charge carriers are separated to the electrodes. The thickness

of the diode is very large, therefore charge carriers rather recombine than travel across the diode. With the higher polarization voltage less skewness is observed in position. The increase of the polarization voltage leads to a larger width of the depletion region. High energy particles have a lower range, therefore they are not able to penetrate deep enough into the thickness of the diode. However, with higher voltages the probability of reaching the depletion region is higher, therefore we can see more charge generation that can be detected by electrodes.

5.0.2 Position distribution

Moving on to discussion about the position distribution detected both with the BET-C system and oscilloscope. The BET-C system was able to measure the position distribution for all the ions that were used, except the carbon one due to its low energy. The configuration of the wires was changed throughout the measurements in order to establish the correct connections for each position. For this reason the position measured with BET-C will differ from the calculated position with oscilloscope data. Both with BET-C and oscilloscope measurement we can see the skewness in the y-direction; in other words the charge collection on the bottom layer had some uncertainties. According to the measurements performed with the BET-C system the skewness seems to be stronger in the middle of the electrode than in the corners. Similarly to the conclusions derived for the carbon beam data, it can be implied that the thickness of the diode is quite high leading to recombination of the charge. In addition, the bottom layer collects holes that have lower mobility in silicon, therefore even more charge never reaches the electrode [14].

Full depletion of the diode requires high voltage, specifically around 180V. With this voltage the current inside the diode would exceed the safety threshold and the diode might get damaged. For this reason the bias was kept between voltage range of 90V and 100V. Polarization of the diode was not complete, leading to uneven distribution of the electric field. Since the charge tends to drift rather in corners than in the middle, the effect can be explained by phenomena called edge effect when the distribution of the charge concentrates in the where the curvature is high leading to increased local electric field [15].

Regarding the position calculation with the oscilloscope measurements the correction function for position calibration functions were found. We can again observe the shift in both y and x-directions but it is clearly stronger in y-direction, due

to the thickness of the diode. Ideal charge distribution would be between 0 and 1 although in reality it is between 0.05 and 0.9 for x-direction. and 0.075 and 0.8 for y-direction. In addition, if we take a look at the calibration graph of x-direction, we can observe that the intersection point between the two graphs is shifted to the left. This is due to asymmetry in the placement of the diode. When the grid is attached to the detector head, the holes are a little bit closer to the right electrode than to the left. The same phenomenon could explain a small shift of intersection point, but the verification of that is impossible.

In the Fig. 21 the position distributions for each ion can be observed. The ion with lowest energy has a more clear distribution with only few outliers than the position distribution for higher energy ions. The outliers that can be observed are caused by the unfiltered pile ups, which cause false signal amplitude leading to a biased position distribution. Most of the pile ups were filtered before calibration, but as we can observe some of those got unnoticed.

Another phenomenon that may be observed, especially in the case of aluminium ion beams, is that charge creates a false row of particles hit on the left side of the diode. This occurs due to asymmetry in the placement of the diode in front of the window on a BET-C rack. The grid is attached to that window, therefore that particle flow happens through it. If we take a look at the Fig. 2, we can see that the left side electrode is closer to the border of the window, while the opposite right side electrode is slightly closer to the centre. If we look at the beam from the device under test point of view, the electrode that is closer to the centre is on the left hand side, where the charge collection seems peculiar. What happens to the charge, when the particle strikes closer to the left electrode, is that it gets collected immediately at the closest electrode and only a very low part of the signal travels to the opposite electrode. Since the signal is very low the recombination rate is much higher therefore almost none of it makes it to the opposite electrode leading the observer to believe the particle strike was closer to the electrode that it actually was.

6 Conclusions

In conclusion, the software part of the BET-C system needs to be re-evaluated due to inconsistencies between the previous result compared to the results established in this work. During the test campaign at UCL the software often crashed and did not save measurement results as it should have done.

With higher energy beams the errors in the system were more frequent than with lower energy ones. In addition, when performing measurements with the software, it is better to wait around 2 to 3 minutes for the diode to stabilize after polarization. This will eliminate the risk of unwanted noise in the beginning of the measurement.

Another aspect that is good to take into account when examining the beam distribution with BET-C system, is that the polarization voltage should be high enough. With BET-C it was observed that the measured distributions were less skewed with 100V than 90V. The position distributions that are presented in Fig. 20 are measured with 100V and some skewness can still be observed. This may be improved with polarizing diode with even higher voltage with limitations at 180V when diode reaches the breakdown.

This diode is designed to collect electrons on the top level and holes on the bottom level. The thickness of the diode is 800µm which is quite large for holes to travel all the way, in order to be collected at the bottom side electrodes. During the drift to the electrodes, charge gets partially recombined, causing signal loss and leading to inaccuracies in detection [12]. In addition, holes have lower carrier mobility than electrons, therefore collection of electrons at the bottom would lead to more accurate results as less charge would be lost [14]. With a lower loss of charge, energy and position would be more precise. During the measurements it was established that charge collection at the top level is more efficient than the bottom level.

Testing the equipment with a range of different energies made it possible to determine the detection range of the BET-C system. The diode has a clear limitation at low energies, when the signal is detected only on the top level electrodes and not the bottom. Because of this, the calculation of position is impossible, therefore the distribution of the beam is not observed. This phenomenon was observed with

the californium-252 source, that has an energy around 5MeV and also with the carbon beam that has energy of 131 MeV. This leads us to the conclusion that the lower energy that was detected so far is the energy of aluminium which is 250 MeV. Also, the upper limit was confirmed during the measurements. In the case of xenon the energy is 995 MeV, which is very close to the limitation provided by the manufacturer which is 1 GeV. With the xenon ion beam the signal that was detected had unexpectedly low voltage transients which can be observed in Fig. 9.

The distribution of the beam is observed with high skewness with BET-C. The reason for that is too low polarization voltage and algorithm of defining the edge of pulse height. We observed with post processing calculations that the approach adopted for finding the value of X, X', Y, Y' has a big impact on the position distribution. The comparison of the two approaches is presented in Fig. 13 and Fig. 12.

Regarding the post-processed data that is extracted with an oscilloscope, the position calibration gives good results for all the ions, regardless of the fact that functions were determined by using only one ion. In table 5 we can observe the average distance of a calibrated position of a particle to its physical position for each ion. The lowest distance is for nickel, since the calibration was performed with it. However, values for other ions are close to the value of nickel. In addition, it can be seen that the diode is placed slightly asymmetrically in front of the grid. This may also affect charge collection, since one electrode is closer to the holes of the grid than the other, leading to almost full signal collection on one side, and almost none at the other side due the charge loss.

7 Future work

During this work not all planned updates were implemented, therefore leaving room for improvement in the BET-C system. For a better understanding of detection limitations it would be useful to test the system with ion beams with energies in the range between 131-250 MeV with a high bias (130-150V). The same goes for the highest detected energy. The system should be tested again with xenon ion beam, in order to conclude if the inaccuracy was due to the limitations in detection or random error. For the post processing of a signal, a better algorithm for pile up filtering should be introduced.

Due to the established uncertainty of the diode caused by its thickness, it is discussed to acquire a new diode with similar technology but considerably lower thickness. Similar characterization process should be made for the new diode to establish its compatibility with the BET-C system.

Regarding ADENEO software a lot of improvement should be made. The software often crashes or slows down when the energy of the examined ion is close to the upper limitation of 1 GeV. When the software crashes the data from the run is not saved automatically, which could be implemented in order to secure the test results. Management of the X and Y graphs by the user is not possible at the moment. The modifications regarding that could be implemented as well. The energy that is displayed in the software often shows incorrect values, even though the distribution on the graph is correct. This as well could be investigated, so that the mean distribution corresponded to the distribution on the graph. In order to change the parameters in the system it is required to depolarize the diode and turn off the preamplifiers. The process takes multiple minutes which slows down the measurements. This may be modified as well along with the securing slow dipolarization of the diode in case of crash. The diode needs stabilization in the beginning of the measurements. This could be taken in account in upgrades of the software. Finally, the total ionizing dose calculation could be implemented in the software in order to reassure, along with energy and beam distributions that dosimetry requirements are fulfilled.

References

[1] R. Gaillard. "Single Event Effects: Mechanisms and Classification". Ch. 2 (2011). Ed. by M. Nicolaidis, pp. 27–52. DOI: 10.1007/978-1-4419-6993-4.

[2] J. R.Letaw. "Single event effects rate predictions in space". *Nuclear Instruments and Methods in Physics Research Section B: Beam Interactions with Materials and Atoms* 56-57 (1991), pp. 1260–1262. DOI: 10.1016/0168-583X(91)95146-5.

[3] A.Gil. "Hale cycle and long-term trend in variation of galactic cosmic rays related to solar rotation". *Astronomy and Astrophysics* 599 (2017), pp. 1–6. DOI: 10.1051/0004-6361/201629604.

[4] J. David. "Spallation, cosmic rays, meteorites, and planetology". *Progress in Particle and Nuclear Physics* 109 (2019). DOI: 10.1016/j.ppnp.2019.103711.

[5] ESCC. "Single Event Effects Test Method And Guidlines". *ESCC Basic Specification No. 25100* 2 (2014).

[6] M.Solal. "A silicon continuous position sensitive diode and associated electronics: modelling and simulation". *Nuclear Instruments and Methods in Physics Research Section A: Accelerators, Spectrometers, Detectors and Associated Equipment* 477 (2002), pp. 491–498. DOI: 10.1016/S0168-9002(01)01788-0.

[7] C. Hu. "PN and Metal–Semiconductor Junctions". Ch. 4 (2009), pp. 89–145.

[8] P. Allport. "Applications of silicon strip and pixel-based particle tracking detectors". *Nature Reviews Physics* 2 (2019). DOI: 10.1038/s42254-019-0081-z.

[9] "Beam Evaluating Tool". *Internal CNES report* (2018).

[10] P. Wilson. "Active components". Ch. 4 (2018), pp. 145–187. DOI: 10.1016/C2010-0-66361-9.

[11] scikit-learn (). URL: https://scikit-learn.org/stable/ (visited on 08/21/2024).

[12] R. Axtmann. “The pulse height defect in semiconductor detectors”. *Nuclear Instruments and Methods in Physics Research* 32 (1965), pp. 70–76. DOI: 10.1016/0029-554X(65)90477-5.

[13] G. Lindstrom. “Radiation hardness of silicon detectors — a challenge from high-energy physics”. *Nuclear Instruments and Methods in Physics Research* 426 (1999), pp. 1–15. DOI: 10.1016/S0168-9002(98)01462-4.

[14] C. Hu. “Motion and Recombination of Electrons and Holes”. Ch.2 (2009), pp. 35–55.

[15] D. K. Cope. “The edge effect for planar electrode”. *Journal of Electroanalytical Chemistry* 439 (1997). DOI: 10.1016/S0022-0728(97)00367-7.